energies

MDPI

Article

Synthesis of BiF_3 and BiF_3-Added Plaster of Paris Composites for Photocatalytic Applications

V. P. Singh [1,2,†], Mirgender Kumar [3,†], Moolchand Sharma [1], Deepika Mishra [4], Kwang-Su Seong [3], Si-Hyun Park [3,*] and Rahul Vaish [1,*]

1 School of Engineering, Indian Institute of Technology Mandi, Suran 175005, HP, India; vinay.phy@gmail.com (V.P.S.); sharma.moolchand09@gmail.com (M.S.)
2 Department of Physics, Government Engineering College, Bharatpur 321001, RJ, India
3 Department of Electronics Engineering, Yeungnam University, Gyeongsan 38541, Korea; mkumar@ynu.ac.kr (M.K.); kssung@ynu.ac.kr (K.-S.S.)
4 Department of Physics, Sri Satya Sai University of Technology & Medical Sciences, Sehore 466001, MP, India; vinay.matsci@ymail.com
* Correspondence: sihyun_park@ynu.ac.kr (S.-H.P.); rahul@iitmandi.ac.in (R.V.)
† First and second authors are equally contributed.

Abstract: A BiF_3 powder sample was prepared from the purchased Bi_2O_3 powder via the precipitation route. The photocatalytic performance of the prepared BiF_3 powder was compared with the Bi_2O_3 powder and recognized as superior. The prepared BiF_3 powder sample was added in a plaster of Paris (POP) matrix in the proportion of 0%, 1%, 5%, and 10% by wt% to form POP–BiF_3(0%), POP–BiF_3(1%), POP–BiF_3(5%), and POP–BiF_3(10%) composite pellets, respectively, and activated the photocatalytic property under the UV–light irradiation,in the POP. In this work, Resazurin (Rz) ink was utilized as an indicator to examine the photocatalytic activity and self-cleaning performance of POP–BiF_3(0%), POP–BiF_3(1%), POP–BiF_3(5%), and POP–BiF_3(10%) composite pellets. In addition to the digital photographic method, the UV–visible absorption technique was adopted to quantify the rate of the de-colorization of the Rz ink, which is a direct measure of comparative photocatalytic performance of samples.

Keywords: BiF_3 nanostructure; POP composite; photocatalyst; Rz ink

Citation: Singh, V.P.; Kumar, M.; Sharma, M.; Mishra, D.; Seong, K.-S.; Park, S.-H.; Vaish, R. Synthesis of BiF_3 and BiF_3-Added Plaster of Paris Composites for Photocatalytic Applications. *Energies* **2021**, *14*, 5159. https://doi.org/10.3390/en14165159

Academic Editor: Wasim Khan

Received: 29 June 2021
Accepted: 14 August 2021
Published: 20 August 2021

1. Introduction

Recent development has focused on creating newly sustainable, low-cost photocatalytic materials with a superior performance than the traditional semiconductor photocatalysts such as TiO_2 and ZnO for self-cleaning applications [1]. In this direction, a huge potential is observed for the Bi-based semiconductors and their complexes [2–11]. This group of materials possess a direct band gap of a wide range from 2.5 eV to 3.2 eV and is severally reported for the fast rate of the creation of photo-induced charge carriers [12,13]. Moreover, most of all the Bi-based compounds show layered structures with polar surfaces and are found responsible for accelerating the separation of photo-generated carriers; consequently, reducing the recombination efficiency and showing a better photocatalytic activity even under the exposure of low intensity of light irradiation [13–17]. Among them, Bi_2O_3has been studied extensively and found to be superior photocatalytic, highly photoconductive, and nontoxic in nature, having a narrow band gap of about 2.8 eV [15,16,18]. Bi_2O_3 has four kinds of polymorphs which are designated as α for the monoclinic structure, β for the tetragonal structure, γ for the body-centered cubic structure, and δ is for the face-centered cubic structure [19,20]. In several cases, Bi_2O_3has been reported for dye degradation, the photosynthesis of organic compounds, and water splitting for hydrogen generation [21–23]. To enhance the photocatalytic performance further, the structure and the surfaces of the Bi_2O_3 compound are tailored extensively. For example, the β phase of

Bi_2O_3 is doped with Ti, which improves the photocatalytic activity comparatively [24]. In some cases, Bi_2O_3 has been further modified to form Bi_2O_3-based complexes with several other materials to create heterojunctions, which further supported the creation and separation of the photo-induced charge carriers in the heterointerface [25–28]. In previous reports, Singh et al. demonstrated the modification of Bi_2O_3 or Bi-based compounds through halogenations which lead to the formation of BiOCl and BiOF compounds, respectively, with a huge advancement in photocatalytic and self-cleaning properties [29,30].

Similarly, in the present work, Bi_2O_3 powder is used as the initial material and processed further with HF treatment and completely modified into the β phase of BiF_3. Usually, BiF_3 exists in two structures, cubic and orthorhombic, depicted as the α phase and β phase, respectively [31]. The α phase of BiF_3 and its applications are reported most commonly for simple synthesis methods and low cost with high photo-activity [32–34]. In a reported research work by Chenkai Feng et al., the α phase of the BiF_3 sample is prepared and then the photocatalytic performance is compared with the commercially available TiO_2 powder sample [32]. Interestingly, the α phase of BiF_3 is found 2.1 times superior to the TiO_2 powder sample [32]. However, the preparation and applications of BiF_3 having β phase are less explored. Therefore, in this work, after the preparation of the β phase of BiF_3, we analyzed its photocatalytic property and compared it with the initially purchased Bi_2O_3powder. In order to explore the possible utilization of BiF_3 for commercial application, it is important to look into a sustainable strategy. One of the methods could be in composite paints and coatings. BiF_3 can be physically mixed with any well-known and widely used materials, such as cement-based paints and other ceramic coatings. Plaster of Paris is known for the aesthetics and decoration material. It is also used in medicine to make casts for broken bones. To explore photocatalysis-based effects in plaster of Paris, it may be used for air cleaning as well as antibacterial properties. Hence, BiF_3 embedded in a plaster of Paris (POP) matrix is fabricated by varying the BiF_3 amounts from 0% to 10 wt%. Further, these POP-BiF_3(%) compositions are tested for the photocatalytic response on Resazurin (Rz) ink. Rz ink is used as a prototype carcinogenic pollutant and an indicator of photocatalytic performance.

2. Materials and Methods

In the process of making POP-BiF_3(%) composites, first, we prepared the powder of the BiF_3 sample. We obtained a precipitation technique to prepare the BiF_3 sample. The fixed amount (5 g) of pure Bi_2O_3 powder of AR grade (Hi-media, ≥99%) was dissolved in the hydrofluoric (HF) acid (Qualikems 40%, Vadodara, India) solution (30 mL) and stirred for 30 min. Under the stirring with HF solution, the yellow color of Bi_2O_3 gradually changed into white-color powder. The product of white powder was washed in distilled water several times followed by acetone and dried at 80 °C for 24 h in a vacuum oven. A fraction of the sample was collected for testing, named sample Bi_2O_3-HF-1. Again, the remaining product of white powder of Bi_2O_3-HF-1 sample was dissolved in the concentrated HF solution and stirred for 30 min. The output product obtained after the second treatment from HF solution was followed with the same procedures of washing, filtering, and drying as for the sample Bi_2O_3-HF-1, and we procured the test sample2 named as sample Bi_2O_3-HF-2. Similarly, a test sample3 was procured and named as sample Bi_2O_3-HF-3 for further testing.

Next, by using the Bi_2O_3-HF-3 powder sample, we prepared POP-BiF_3(%) composite pellets. In the composites, we maintained the concentration of Bi_2O_3-HF-3 powder in the POP matrix in accordance with 0, 1, 5, and 10 by wt%. With respect to each composition of POP-BiF_3(%) composites, the calculated amount of Bi_2O_3-HF-3 powder sample and POP were mixed rigorously to prepare a homogeneous mixture, separately. The paste of each mixture of different POP-BiF_3(%) composites was obtained by adding an equal amount of distilled water. Individually, the paste of different POP-BiF_3(%) composites was transferred into cylindrical molds of 20 mm diameter and 10 mm height to prepare the pellets of each composition, respectively. Finally, the pellets were left to naturally dry fortwo days.

The structural analysis of Bi_2O_3, HF-treated Bi_2O_3 test samples, and POP-BiF_3(%) composite pellets was performed through X-ray diffraction (XRD) (Rigaku), having 9 kW rotating anode and Cu Kα source. Microstructure analysis was obtained from FE-SEM (Inspect™S50). Optical property and photocatalytic performance were tested via UV–visible spectrophotometer of double beam (Thermo Scientific, Evolution 220, Waltham, MA, USA). In addition, to carry out the photocatalytic reaction, we used a box inbuilt with a lamp (Hitachi FL8BL-Blight) as a UV light source having maximum emission ~355 nm wavelengths. The distance between the lamps and the samples was adjusted such that the intensity falling on the samples was maintained at about ~3200 lx.

3. Results and Discussion

The systematic XRD results of Bi_2O_3 and the samples obtained from the successive fluorination of Bi_2O_3 via HF solution are shown in Figure 1. The step-wise fluorinated samples are denoted as Bi_2O_3-HF-1, Bi_2O_3-HF-2, and Bi_2O_3-HF-3, respectively. XRD of the purchased Bi_2O_3 sample was compared with the JCPDS file no 76–1730 and matched with the monoclinic phase. XRD results of the Bi_2O_3-HF-1 sample revealed that after the 1st washing of Bi_2O_3 powder, new diffraction peaks appeared in the X-ray diffraction pattern. A set of these new diffraction peaks was related to the intermediate phase of $Bi_{1.2}F_{2.4}O_{0.6}$(PDF-36-0457), which are marked as '*'. The other set of remaining peaks with less intensity belongs to the orthorhombic structure of BiF_3 (PDF-70-2407). XRD results of the Bi_2O_3-HF-2 sample for a 2nd consecutive washing of the Bi_2O_3 powder showed the relative increase in the intensity of diffraction peaks belonging to the BiF_3 (PDF-70-2407) phase structure at the expense of the diffraction peaks belonging to an intermediate phase of $Bi_{1.2}F_{2.4}O_{0.6}$ (PDF-36-0457), relatively. The almost pure phase of BiF_3 (PDF-70-2407) appeared after the 3rd consecutive washing of Bi_2O_3 powder in addition to a very small quantity of an unidentified impure phase which is marked as '#'. Thus, multiple washing of Bi_2O_3 powder through the concentrated HF solution led towards the formation of the almost pure orthorhombic structure of the BiF_3 powder sample.

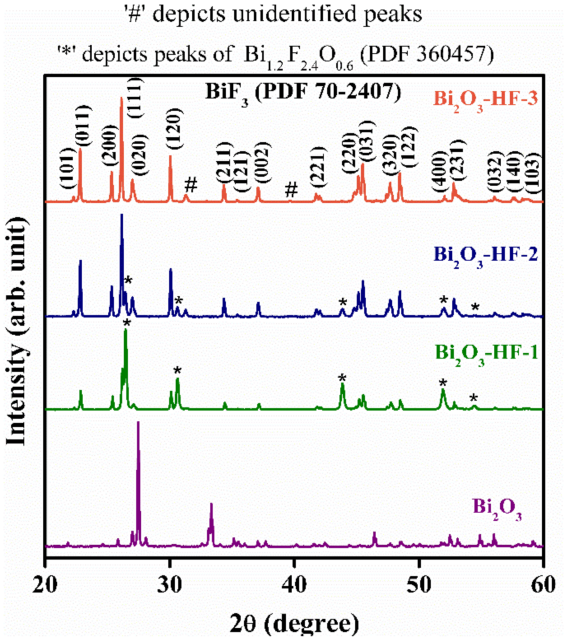

Figure 1. X-ray diffraction patterns of purchased Bi_2O_3 and Bi_2O_3 after three successive HF treatments depicted as Bi_2O_3-HF-1, Bi_2O_3-HF-2, Bi_2O_3-HF-3, and Bi_2O_3-HF-4, respectively.

Only a few solution techniques have been used for the formations of various phases of the BiF_3 sample through different methods. For example, Feng et al. reported the formation of BiF_3 (JCPDS: 51-0944) by a simple water-bath method, where they kept the molar ratio of

Bi and F above 1:3, otherwise the impurity of Bi_2O_3 and BiOF remained present [32]. In this method, the constituent of Bi was obtained from Bi_2O_3 while the element of F was attained from the NH_4F solution [32]. Zhao et al. reported the evolution of the BiF_3 nanocrystals in various shapes from monodispersed nano-plates to nano-rods and then to nanowires via the novel acid–base couple extraction route and tuning the molar ratio of F vs. Bi [31]. Sarkar et al. used Poly (vinyl pyrrolidone) (PVP) for the encapsulation and formation of cubic nanocrystals of BiF_3 via the hydrothermal method [35]. In another method, by using a novel ion-exchange approach, Kan et al. produced pure BiF_3 (JCPDS: 73-1988). Here, the NH_4F solution was used for the constituent of F while BiOCl was utilized to attain the element of Bi in accordance with the molar ratio (RF = F/Bi) of 8:1 [36]. Below to the molar ratio of 8:1 (RF), the final product consisted of a small amount of $Bi_7F_{11}O_5$ as an impurity phase [36].

Contrary to the above reported studies, in the present method, the ratio of O/F was controlled via a chemical bath of Bi_2O_3 in a concentrated HF solution. The constituent of Bi was extracted from the powder of Bi_2O_3, while for the element of F in a concentrated HF solution was utilized. Bi_2O_3 powder was washed several times from the concentrated HF solution, which may have led to two types of products, as follows in the reaction mechanisms one and two given below:

$$2Bi^{3+} + 6F^{-} \rightarrow 2BiF_3 \rightarrow \text{(Concentrated HF)} \quad (1)$$

$$2Bi^{3+} + 2H_2O + 6F^{-} \rightarrow 2BiOF\downarrow + 4HF \text{ (Diluted HF)} \quad (2)$$

Multiple washing from HF solution increased the constituent of F and led towards the formation of BiF_3 from Bi_2O_3 powder. Normally, if the Bi_2O_3 powder is washed from the concentrated HF solution, the positively charge Bi^{3+} ion reacts with F^{-} ion and forms BiF_3 and follows reaction mechanism one. However, in the HF solution, some water content always remains present; therefore, in the case of the 1st washing, some of the Bi_2O_3 powder converted into BiF_3 according to reaction mechanism one, while some of the Bi_2O_3 powder reacted with HF as well as the water content, followed reaction mechanism2 and formed an intermediate product of the BiOF family, which was recognized as $BiO_{0.51}F_{1.98}$ in the present case. Further, the 2nd and 3rd washing provided more and more F^{-} ion in the solution which again reacted with the intermediate product of $BiO_{0.51}F_{1.98}$ and converted it to the final product of the BiF_3 sample. Multiple washing and high concentrations of HF increased the F concentration in the O/F ratio and led toward the cubic-αBiF_3 phase (PDF-073-1988) from the Bi_2O_3 powder.

Further, the BiF_3 powder was investigated for its photocatalytic performance and compared with the Bi_2O_3 powder sample. A total of0.05 g powder of both Bi_2O_3 and BiF_3were sonicated in 50-50 mL water solutions of the hazardous dye of Methylene blue (MB), separately, as test solutions. Before the photocatalytic investigation of Bi_2O_3 and BiF_3 samples, to neglect the effect of the adsorption–desorption of the dye over the surfaces of these powders, first both the test solutions of Bi_2O_3 and BiF_3 in MB were sonicated under dark for a 30 min duration to achieve the adsorption–desorption equilibrium. Then, both the test solutions were transferred under the UV light irradiation of a 355 nm wavelength. To probe the photocatalytic activity of the Bi_2O_3 and BiF_3 powder samples, 1-1 mL of the MB was collected in a separate Eppendorf from both the test solutions at fixed time intervals. Finally, the absorption study of the collected samples was carried out by using a UV–visible spectrophotometer. After the fixed time of reaction, both the solutions were sonicated for five minutes to maintain the homogeneity and, then, 1-1 mL of the MB was collected. Each collected sample was centrifuged to remove the segregated residual from the solutions. At last, the photocatalytic decomposition of MB for each collected sample from both the set of solutions immersed with Bi_2O_3 and BiF_3 powders were tested from UV–visible spectroscopy, respectively.

The adsorption–desorption reaction analysis for both the samples under the dark environment showed an insignificant change in the concentration of MB solutions (absorbance

results probed by UV–visible spectroscopy is not shown here). After adsorption–desorption, the photolysis and photocatalytic results of decomposition, as well as the kinetic rate of the decomposition of MB solutions under UV exposure, were plotted and represented in Figure 2a–c. The decomposition of the MB solution probed via absorbance data of UV–visible spectroscopy confirmed a fast degradation of MB solution for the BiF_3 powder sample as compared to the Bi_2O_3 powder. For comparison purposes, and to remove the artifacts during the photocatalytic reaction, the photolysis of the blank MB solution was obtained for the same parameters and for the same time scale as maintained for the photocatalytic decomposition of MB solutions for the Bi_2O_3 and BiF_3 powder samples. A control reaction of photolysis of blank MB solution under the exposure of 355 nm light radiation showed a negligible change in the concentration. In Figure 2d,e, the Co stands for initial concentration, while Ct represents the time-dependent concentration of the MB solution after the photocatalytic decomposition. Using the parameters Co and Ct and their relation with time, i.e., $\ln(C/Co) = k_f\, t$, the decomposition rate constant of MB solutions due to the photocatalytic reaction for both the powder samples were calculated and compared. Here, k_f represents the rate constant of photocatalytic reactions, which was calculated as 0.0011 and 0.0103 min^{-1} for the Bi_2O_3 and BiF_3 powders, respectively. Thus, the photocatalytic degradation of the BiF_3 powder sample was confirmed to be multiple times higher than the Bi_2O_3 powder sample. A comprehensive study of photocatalysis is shown in Table 1.

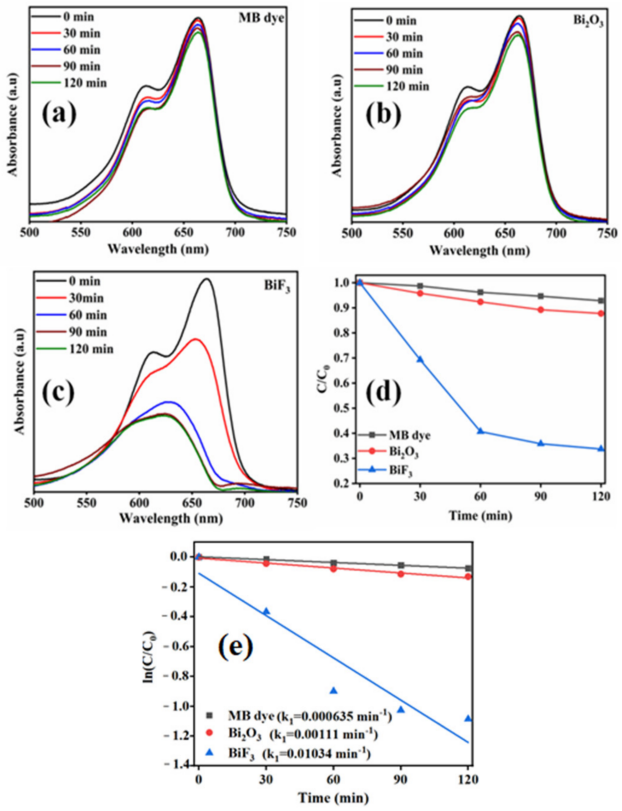

Figure 2. Absorption vs. wavelength spectra for (**a**) the photolysis of Methylene blue (MB), and the photocatalysis of MB under the exposure of UV light of 355 nm wavelength due to (**b**) Bi_2O_3powder and (**c**) BiF_3 powder (**d**) respective C/Co vs. time plots, and (**e**) ln(C/Co) vs. time plots to obtain the pseudo-first-order reaction rate constant for the photolysis of MB and the photocatalysis of MB.

Four different composite pellets of POP–BiF_3(%) were obtained. The BiF_3 power was varied in the POP matrix in accordance with 0, 1, 5, and 10 by wt%. Here, the pellets of POP–BiF_3(%) composites were named as POP–BiF_3(0%), POP–BiF_3(1%), POP–BiF_3(5%), and POP–BiF_3(10%), respectively. The composite formation and purity of POP–BiF_3(0%),

POP–BiF_3(1%), POP–BiF_3(5%), and POP–BiF_3(10%) pellets were checked and verified through XRD (not shown here).

Again, the absorption of UV–visible radiation for POP–BiF_3(0%), POP–BiF_3(1%), POP–BiF_3(5%), and POP–BiF_3(10%) pellets was probed and utilized for the bandgap calculations according to the Kubelka–Munk model [37]. Results are shown in Figure 3a,b. Figure 3a demonstrates the gradual increase in the absorption from the visible to UV region for the POP sample. Adding BiF_3 in the POP matrix improved the absorption towards the visible range, relatively. The results of the absorption coefficient (α) vs. incident photon energy E (hν) obtained from Figure 3a were extrapolated according to the Kubelka–Munk model to calculate the direct bandgap of POP and POP–BiF_3(%) composites, as shown in Figure 3b. Results showed that the bandgap tended to decrease with the addition of BiF_3 in the POP matrix from 3.69 eV to 3.26 eV, respectively.

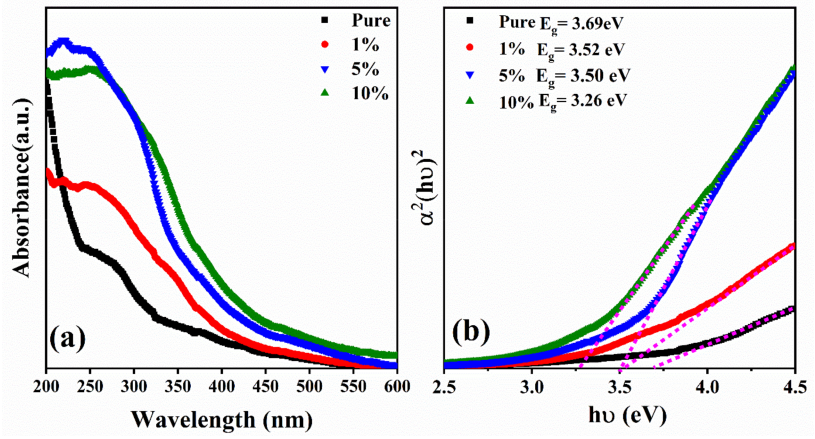

Figure 3. (**a**) Absorption spectra and (**b**) $\alpha^2(h\nu)^2$ vs. hν plots for the band gap (E_g) calculation of POP–BiF_3 (%) composites with the variation of BiF_3 concentration 0%, 1%, 5%, and 10% in POP matrix.

The variation in morphology of the POP–BiF_3(%) composite pellets along with the change of BiF_3 concentration in the POP matrix were probed through SEM and are shown in Figure 4a–d. The surface image of POP–BiF_3(0%) pellet stands for the pure POP sample and shows a homogeneous rod-shape microstructure. These rods were entangled with each other and made net-like porous surfaces. One end of the rod was defused in the surface while the other end seemed to emerge from the surface and dangle. Such entangled rods over the surface of the POP–BiF_3(0%) pellet were due to water treatment and the continuous hydration of POP which led to the continuous nucleation and growth of rods in random orientations. SEM images of the BiF_3-added POP–BiF_3(0%), POP–BiF_3(1%), POP–BiF_3(5%), and POP–BiF_3(10%) composite pellets revealed almost similar surfaces to the POP–BiF_3(0%) pellet accompanied with several entangled random oriented rods forming the net-like porous structure. However, with the addition of BiF_3 in the POP matrix, the porosity of the surface reduced in POP–BiF_3(1%), POP–BiF_3(5%), and POP–BiF_3(10%) composite pellets, relatively, as compared to the surface of the POP–BiF_3(0%) pellet. The addition of BiF_3 may have filled the pores of POP and, therefore, led to a smooth and glassy surface in the POP–BiF_3(10%) composite pellet.

Further, to check the photocatalytic performance of BiF_3 in the POP matrix, the Rz ink was prepared by using a known reported method [38]. Rz ink is an indicator of self-cleaning/photocatalysis, which changes its color if coated over any surface of photocatalytic material under the exposure of UV irradiation. Therefore, an equal amount of ink was pasted over each surface of POP–BiF_3(0%), POP–BiF_3(1%), POP–BiF_3(5%), and POP–BiF_3(10%) composite pellets. These pellets were subjected to UV light (355 nm) illumination with equal exposures and monitored with time on several fixed intervals for 180 min of time duration. Each time, surface images of POP–BiF_3(0%), POP–BiF_3(1%),

POP–BiF_3(5%), and POP–BiF_3(10%) composite pellets were obtained via a high-quality digital camera. For comparison purposes, all captured images on certain time intervals were compiled together and shown in Figure 5. In correlation to Figure 5, ΔRGB't vs. time is plotted and shown as Figure 6a,b, which represents the change in blue as Figure 6a and change in red color as Figure 6b due to photo-reduction in the Rz indicator ink under the UV light irradiation on POP–BiF_3(%) composites, respectively.

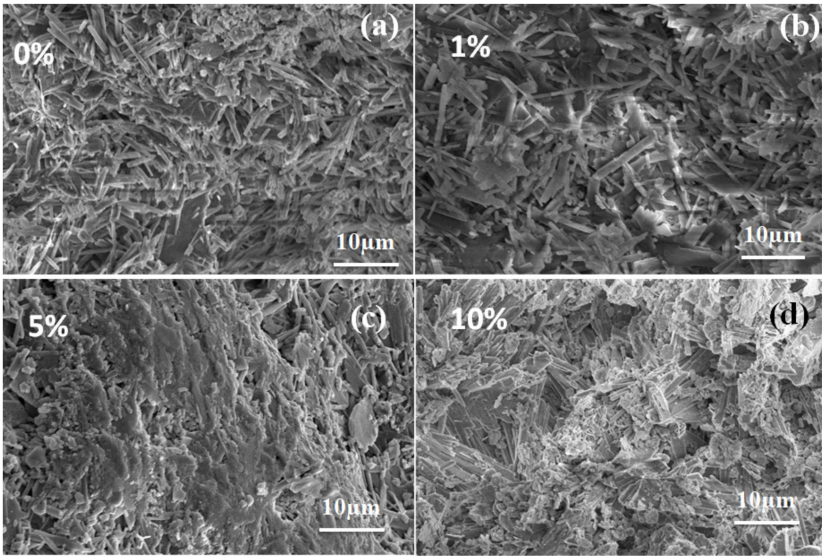

Figure 4. Typical SEM images of POP–BiF_3 (%) composites along with the concentration variation of BiF_3 for (**a**) 0%, (**b**) 1%, (**c**) 5%, and (**d**) 10% in POP matrix.

Table 1. Comprehensive study of photocatalysis activity of BiF_3 catalyst.

Catalyst	Process	Pollutant	Power Source	Catalysis Time	Performance
BiOI/BiF_3 composite [39]	Photocatalysis	Tetracycline hydrochloride	Visible light	120 min	~75.6%
BiF_3−Bi_2NbO_5F core−shell [34]	Photocatalysis	RB dye	Visible light	90 min	0.028 min^{-1}
BiOCl/BiF_3 heterojunction [40]	Photocatalysis	MO dye	UV light	30 min	~90%
BiF_3 octahedrons [41]	Photocatalysis	RB dye	Solar light	50 min	~95.7%
BiF_3 nanoparticles [32]	Photocatalysis	RB dye	UV light	50 min	~78.5%
BiF_3/BiOBr heterojunctions [42]	Photocatalysis	MO dye	Visible light	200 min	~82.6%
Bismuth Fluoride Surface Crystallized $2Bi_2O_3$-B_2O_3 Glass [43]	Photocatalysis	Rhodamine 6G	Halogen lamp	120 min	~85%
Bismuth Fluoride on SrO-Bi_2O_3-B_2O_3transparent Glass ceramic [44]	Photocatalysis	MB dye	Visible lights	540 min	0.02226 min^{-1}
BiOCl/BiF_3 on ZnO–Bi_2O_3–B_2O_3 glass [45]	Photocatalysis	MB dye	UV light	300 min	~90%
BiF_3 (present study)	Photocatalysis	MB dye	UV light	120 min	0.0103 min^{-1}

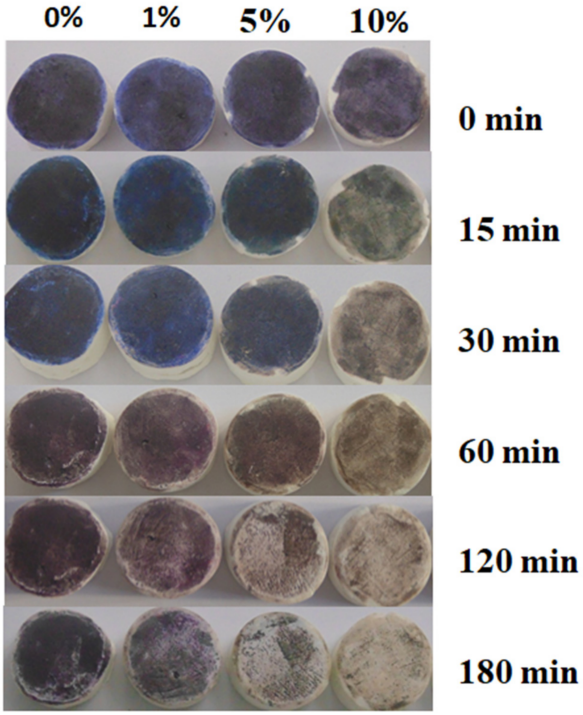

Figure 5. Photo-reduction in Rz indicator ink for 3 h reaction timeline on POP–BiF_3 (%) composites having the variation of BiF_3 0%, 1%, 5%, and 10% by wt., respectively, under the exposure of 355 nm wavelength of UV light irradiation.

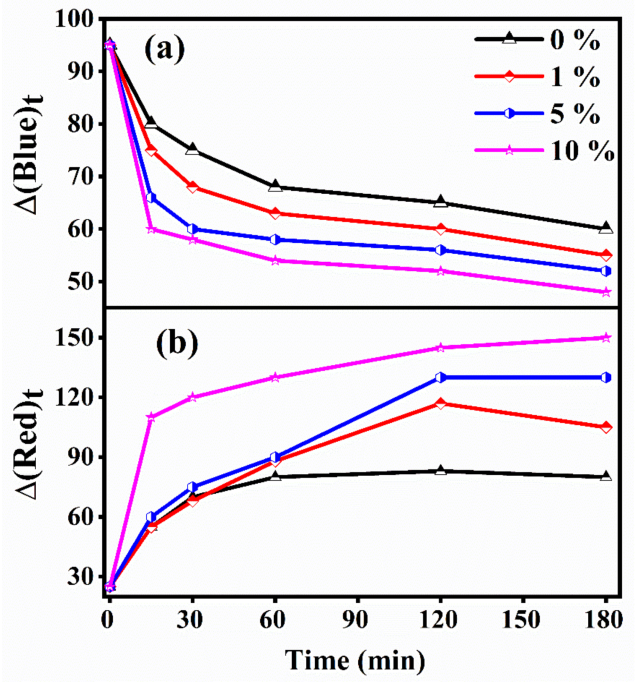

Figure 6. ΔRGB't vs. time plots for (**a**) blue and (**b**) red color change due to photo-reduction inRz indicator ink on POP–BiF_3(%) composites having BiF_3 0%, 1%, 5%, and 10% by wt., respectively, under the UV light irradiation.

In the present case, under the exposure of UV light on the POP–BiF_3(0%) composite pellet, which had no BiF_3 content, showed no color change on the surface up to the 30 min of time duration, while a slight change after 60 min to 180 min was monitored. This slight change from a blue to purple color was due to the photolysis of the Rz ink. For POP–

BiF_3(1%), POP–BiF_3(5%), and POP–BiF_3(10%) composite pellets, the color of the Rz ink readily changed in proportion to the BiF_3 content in POP from royal blue to pink and then into colorless ink. The rate of change in the color of the Rz ink was systematic and increased for POP–BiF_3(0%), POP–BiF_3(1%), POP–BiF_3(5%), and POP–BiF_3(10%) composite pellets, respectively. The color of the Rz ink over the surface of the POP–BiF_3(10%) composite pellet appeared almost colorless within the 180 min time period.

Usually, the rate of the change of color of the Rz ink indicates the rate of photocatalytic reduction. The reaction mechanism of photocatalytic reduction and the color-change of the Rz ink are mentioned as under Equations (3)–(6).

$$BiF_3 \xrightarrow{h\vartheta} BiF_3\left(e^-, h^+\right) \tag{3}$$

$$Glycerol \xrightarrow{h^+} OH + Glyceric\ acid \tag{4}$$

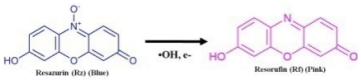

(5)

$$BiF_3 * \left(e^-, h^+\right) \rightarrow BiF_3 \tag{6}$$

At the same time of the image capture, the POP–BiF_3(0%), POP–BiF_3(1%), POP–BiF_3(5%), and POP–BiF_3(10%) composite pellets were again tested through UV–visible spectroscopy for a quantitative analysis of the photocatalytic reduction in the Rz ink coated over the surfaces. Absorption peak intensities corresponding to the photo catalytic reduction were monitored at two different wavelengths, i.e., 630 nm and 581 nm. The absorption spectra obtained from the UV–visible spectroscopy is illustrated in Figure 7a–d. The peak intensity monitored at the 630 nm wavelength directly correlated to the blue color of the Rz ink and with the exposure of UV light (355 nm). The peak intensity of absorbance decreased at the wavelength of 630 nm along with the color change from blue to pink, resulting in the formation of resorufin (Rf) as a byproduct. The intensity decay of another peak at 581 nm represented the photobleaching of the Rf molecule as and when the color changed from pink to colorless. Under the effect of UV light irradiation, a negligible change in the intensity of characteristic absorption of the Rz ink was observed for the POP–BiF_3(0%) composite pellet; however, the absorption intensity of the Rz ink decreased consistently for all the other samples just in accordance with the color change observed in the digital photographs as shown in Figure 5. The absorption results are shown in Figure 7a–d was further utilized to extract the kinetic rate of photocatalytic reduction and photo mineralization of intermediates of the Rz ink monitored for both the wavelengths at 630 nm and 581 nm, respectively, shown in Figure 8. In Figure 8, Co represents the initial (t = 0) absorbance of the Rz ink and C is the absorbance of the Rz ink, which varied with time t. The Co and C and kinetic rate of photocatalytic reduction was calculated corresponding to the absorption spectra monitored for both the wavelengths of absorbance, i.e., 581 nm and 630 nm of Rz ink. For the POP–BiF_3(0%) sample, the results showed that the intensity decay, as well as the kinetic rate of reaction due to the photocatalytic degradation of the Rz ink corresponding to the wavelengths monitored at 581 nm and 630 nm for 180 min of time duration, was less. Generally, the photocatalytic reaction rate was monitored to correspond faster to the absorbance at 630 nm wavelengths in comparison to the absorbance around the 581 nm wavelength for all samples. As compared to POP–BiF_3(0%), the POP–BiF_3(1%), POP–BiF_3(5%), and POP–BiF_3(10%) composite pellets showed relatively faster kinetic rate of photocatalytic reduction in the Rz ink, respectively.

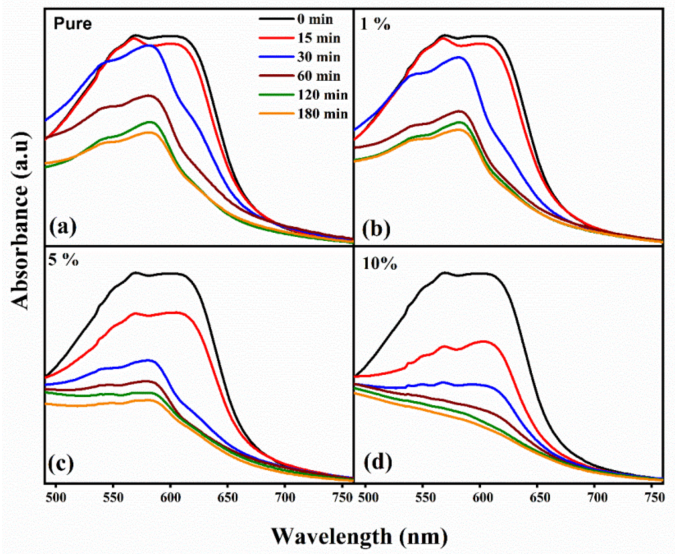

Figure 7. Absorption vs. wavelength spectra for the photocatalysis of Rz ink on the surface of POP–BiF_3(%) composites with the variation of BiF_3 concentration (**a**) 0%, (**b**) 1%, (**c**) 5%, and (**d**) 10% in POP matrix.

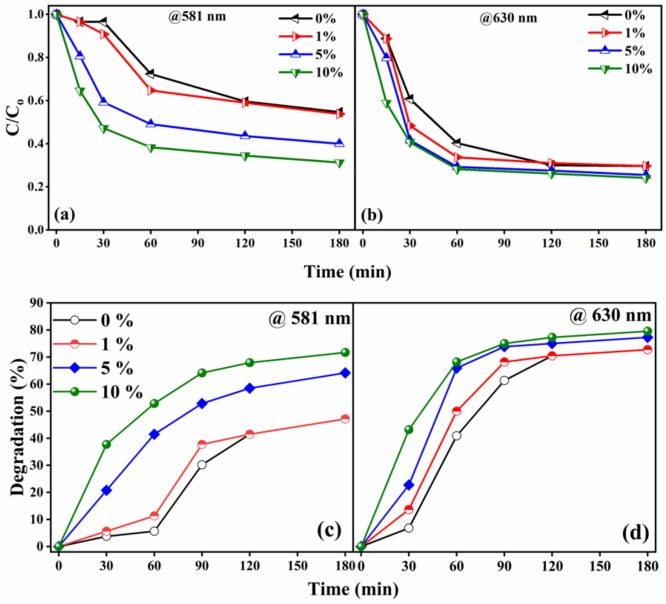

Figure 8. The C/Co vs. time plots for photocatalytic degradation of Rz ink for POP–BiF_3(%) composites monitored at: (**a**) 581 nm and (**b**) 630 nm wavelength, and respective percentage of photocatalytic degradation for (**c**) 581 nm and (**d**) 630 nm wavelength.

For simplicity, the photoreduction due to UV light irradiation of Rz ink, which was coated on POP–BiF_3 composite pellets, is shown in Figure 9. Under the illumination of UV light irradiation, the catalyst material BiF_3 present in POP generated sacrificial donor electrons on its surface which reacted with the photo-induced holes of the Rz ink. Therefore, the glycerol present in the Rz ink utilized this sacrificial donor electron and generated an •OH radicle along with glyceric acid as a by-product. At the same time, these intermediate •OH radicles reduced the blue color of the Rz ink into Rf of the pink color after the long-time illumination of UV light irradiation, resulting in the reduction in the Rf molecule into a colorless product. Similar to the Rz ink, the harmful pollutants may have also reduced into non-harmful products with the aid of hydroxyl radicals generated on the surface of the photocatalytic BiF_3 in the POP matrix. In the present work, we obtained a maximum

content of BiF_3 only up to 10% in the POP matrix. The Further addition of BiF_3 in POP may have led to the decay in the mechanical strength of the architecture. The concentration of BiF_3 inside the POP matrix along with an optimized photocatalytic performance and superior strength of the structures are a further matter of research. Thus, the above results demonstrate the successful photocatalytic application of BiF_3 inside the POP matrix. POP is an important cementitious material used for the making of several building constructions and sculptures. We propose here for the addition of BiF_3 as an activated photocatalytic material in the side of any cementitious material for self-cleaning of building constructions and a reduction in environmental pollution.

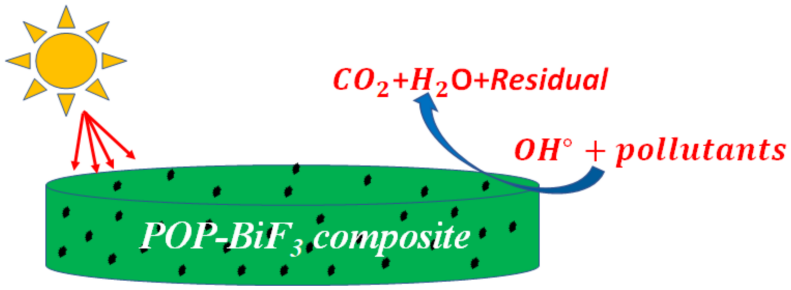

Figure 9. The schematic representation of the proposed mechanism for the photocatalytic degradation of pollutants under UVlight irradiation over POP–BiF_3 composite pellet surfaces.

4. Conclusions

Successfully, theBiF_3 powder sample was prepared via the precipitation route simply by washing the purchased powder of Bi_2O_3 several times into the concentrated HF solution. After several washes through the concentrated HF solution, the Bi_2O_3 powder was systematically transformed into BiF_3 powder in conjunction with each washing. An intermediate phase of $Bi_{1.2}F_{2.4}O_{0.6}$ was identified for the 1st and 2nd washing of the Bi_2O_3 powder, which completely vanished after the 3rd washing and converted into the BiF_3 powder sample. The photocatalytic performance of the as-prepared BiF_3 powder was tested and compared with the Bi_2O_3 powder on a hazardous industrial waste solution of MB dye. The BiF_3 powder rapidly decomposed the MB solution under the visible light illumination as compared to the purchased Bi_2O_3 powder sample. Usually, POP is used vastly in the construction as well as the building of sculptures and, therefore, is always exposed to water as well as air pollutants. Therefore, to check the self-cleaning activity from such pollutants and introduce the photocatalytic properties in POP, BiF_3 powders were added according to 0%, 1%, 5%, and 10% by wt% in the POP matrix. The photocatalytic and self-cleaning properties of these POP–BiF_3 composites were demonstrated by using a well-known photocatalysis indicator ink of Rz under visible light exposure. Due to the photocatalytic effect of POP–BiF_3 composites under the solar illumination, the blue color of the Rz ink turned into Rf of the pink color. The long-time illumination of visible light resulted from the reduction in the pink color Rf molecules into the colorless product. Photocatalytic performances were improved linearly for the incorporation of BiF_3 up to 10% of the concentration in the POP matrix.

Author Contributions: Conceptualization, V.P.S. and R.V.; methodology, V.P.S., R.V., S.-H.P. and M.K.; validation, V.P.S., M.S. and D.M.; formal analysis, V.P.S., M.S. and D.M.; investigation, V.P.S., M.K., M.S. and D.M.; resources, R.V., K.-S.S. and S.-H.P.; data curation, V.P.S. and M.K.; writing, V.P.S., R.V., S.-H.P. and M.K.; writing—review and editing, V.P.S., R.V., S.-H.P. and M.K.; visualization, V.P.S., R.V., S.-H.P. and M.K.; supervision, R.V., K.-S.S. and S.-H.P.; project administration, R.V., K.-S.S. and S.-H.P.; funding acquisition, K.-S.S. and S.-H.P. All authors have read and agreed to the published version of the manuscript.

Funding: This work was supported by the 2021 Yeungnam University Research Grant.

Acknowledgments: V. P. Singh and Rahul Vaish acknowledge the NPIU and AICTE for the CRS grant under the TEQIP III program for research-related work.RV thanks the CSIR, New Delhi, India, for the financial support under the sponsored research project scheme.

Conflicts of Interest: The authors declare no conflict of interest.

References

1. Li, J.; Yu, Y.; Zhang, L. Bismuth oxyhalide nanomaterials: Layered structures meet photocatalysis. *Nanoscale* **2014**, *6*, 8473–8488. [CrossRef]
2. Tian, G.; Chen, Y.; Zhou, W.; Pan, K.; Dong, Y.; Tian, C.; Fu, H. Facile solvothermal synthesis of hierarchical flower-like Bi_2MoO_6 hollow spheres as high performance visible-light driven photocatalysts. *J. Mater. Chem.* **2011**, *21*, 887–892. [CrossRef]
3. Zhang, B.L.W.; Wang, Y.J.; Cheng, H.Y.; Yao, W.Q.; Zhu, Y.F. Synthesis of porous Bi_2WO_6 thin films as efficient visible-light-active photocatalysts. *Adv. Mater.* **2009**, *21*, 1286–1290. [CrossRef]
4. Li, R.; Zhang, F.; Wang, D.; Yang, J.; Li, M.; Zhu, J.; Zhou, X.; Han, H.; Li, C. Spatial separation of photogenerated electrons and holes among {010} and {110} crystal facets of $BiVO_4$. *Nat. Commun.* **2013**, *4*, 1432. [CrossRef]
5. Wang, B.C.; Nisar, J.; Pathak, B.; Kang, T.W.; Ahuja, R. Band gap engineering in $BiNbO_4$ for visible-light photocatalysis. *Appl. Phys. Lett.* **2012**, *100*, 182102. [CrossRef]
6. Shi, R.; Lin, J.; Wang, Y.; Xu, J.; Zhu, Y. Visible-light photocatalytic degradation of $BiTaO_4$ photocatalyst and mechanism of photocorrosion suppression. *J. Phys. Chem. C* **2010**, *114*, 6472–6477. [CrossRef]
7. You, Q.; Fu, Y.; Ding, Z.; Wu, L.; Wang, X.; Li, Z. A facile hydrothermal method to BiSbO4 nanoplates with superior photocatalytic performance for benzene and 4-chlorophenol degradations. *Dalton Trans.* **2011**, *40*, 5774–5780. [CrossRef] [PubMed]
8. Wu, J.; Huang, F.; Lü, X.; Chen, P.; Wan, D.; Xu, F. Improved visible-light photocatalysis of nano-$Bi_2Sn_2O_7$ with dispersed s-bands. *J. Mater. Chem.* **2011**, *21*, 3872–3876. [CrossRef]
9. Gao, F.; Chen, X.; Yin, K.; Dong, S.; Ren, Z.; Yuan, F.; Yu, T.; Zou, Z.G.; Liu, J.-M. Visible-light photocatalytic properties of weak magnetic $BiFeO_3$ nanoparticles. *Adv. Mater.* **2007**, *19*, 2889–2892. [CrossRef]
10. Zhang, Q.; Gong, W.; Wang, J.; Ning, X.; Wang, Z.; Zhao, X.; Ren, W.; Zhang, Z. Size-dependent magnetic, photoabsorbing, and photocatalytic properties of single-crystalline $Bi_2Fe_4O_9$ semiconductor nanocrystals. *J. Phys. Chem. C* **2011**, *115*, 25241–25246. [CrossRef]
11. Pan, C.; Zhu, Y. Size-controlled synthesis of $BiPO_4$ nanocrystals for enhanced photocatalytic performance. *J. Mater. Chem.* **2011**, *21*, 4235–4241. [CrossRef]
12. Lin, X.; Huang, F.; Wang, W.; Shi, J. Photocatalytic activity of $Bi_{24}Ga_2O_{39}$ for degrading methylene blue. *Scr. Mater.* **2007**, *56*, 189–192. [CrossRef]
13. Mohn, C.E.; Stølen, S. Influence of the stereochemically active bismuth lone pair structure on ferroelectricity and photocalytic activity of Aurivillius phase Bi_2WO_6. *Phys. Rev. B Condens. Matter Mater. Phys.* **2011**, *83*, 01410. [CrossRef]
14. Yu, C.; Yang, P.; Tie, L.; Yang, S.; Dong, S.; Sun, J.; Sun, J. One-pot fabrication of β-Bi_2O_3@Bi_2S_3 hierarchical hollow spheres with advanced sunlight photocatalytic RhB oxidation and Cr(VI) reduction activities. *Appl. Surf. Sci.* **2018**, *455*, 8–17. [CrossRef]
15. Yan, Q.; Xie, X.; Liu, Y.; Wang, S.; Zhang, M.; Chen, Y.; Si, Y. Constructing a new Z-scheme multi-heterojunction photocataslyts Ag-AgI/BiOI-Bi_2O_3 with enhanced photocatalytic activity. *J. Hazard. Mater.* **2019**, *371*, 304–315. [CrossRef] [PubMed]
16. Chen, L.; He, J.; Yuan, Q.; Liu, Y.; Au, C.T.; Yin, S.F. Environmentally benign synthesis of branched Bi_2O_3-Bi_2S_3 photocatalysts by an etching and re-growth method. *J. Mater. Chem. A* **2015**, *3*, 1096–1102. [CrossRef]
17. Zou, S.; Teng, F.; Chang, C.; Liu, Z.; Wang, S. Controllable synthesis of uniform BiOF nanosheets and their improved photocatalytic activity by an exposed high-energy (002) facet and internal electric field. *RSC Adv.* **2015**, *5*, 88936–88942. [CrossRef]
18. Lu, H.; Hao, Q.; Chen, T.; Zhang, L.; Chen, D.; Ma, C.; Yao, W.; Zhu, Y. A high-performance Bi_2O_3/Bi_2SiO_5 p-n heterojunction photocatalyst induced by phase transition of Bi_2O_3. *Appl. Catal. B Environ.* **2018**, *237*, 59–67. [CrossRef]
19. Bian, Z.; Zhu, J.; Wang, S.; Cao, Y.; Qian, X.; Li, H. Self-Assembly of Active Bi_2O_3/TiO_2 Visible Photocatalyst with Ordered Mesoporous Structure and Highly Crystallized Anatase. *J. Phys. Chem. C* **2008**, *112*, 6258–6262. [CrossRef]
20. Hameed, A.; Montini, T.; Gombac, V.; Fornasiero, P. Surface phases and photocatalytic activity correlation of Bi_2O_3/Bi_2O_{4-x} nanocomposite. *J. Am. Chem. Soc.* **2008**, *130*, 9658–9659. [CrossRef]
21. Brezesinski, K.; Ostermann, R.; Hartmann, P.; Perlich, J.; Brezesinski, T. Exceptional photocatalytic activity of ordered mesoporous β-Bi_2O_3 thin films and electrospun nanofiber mats. *Chem. Mater.* **2010**, *22*, 3079–3085. [CrossRef]
22. Dai, Y.; Yin, L. Synthesis and photocatalytic activity of Ag-Ti-Si ternary modified α-Bi_2O_3nanoporous spheres. *Mater. Lett.* **2015**, *142*, 225–228. [CrossRef]
23. Naik, B.; Parida, K.M.; Behera, G.C. Facile synthesis of Bi_2O_3/$TiO_{2-x}N_x$ and its direct solar-light-driven photocatalytic selective hydroxylation of phenol. *ChemCatChem* **2011**, *3*, 311–318. [CrossRef]
24. Yin, L.; Niu, J.; Shen, Z.; Chen, J. Mechanism of reductive decomposition of pentachlorophenol by ti-doped β-Bi_2O_3 under visible light irradiation. *Environ. Sci. Technol.* **2010**, *44*, 5581–5586. [CrossRef] [PubMed]
25. Zhao, W.; Zhang, J.; Zhu, F.; Mu, F.; Zhang, L.; Dai, B.; Xu, J.; Zhu, A.; Sun, C.; Leung, D.Y. Study the photocatalytic mechanism of the novel Ag/p-Ag_2O/n-$BiVO_4$ plasmonic photocatalyst for the simultaneous removal of BPA and chromium(VI). *Chem. Eng. J.* **2019**, *361*, 1352–1362. [CrossRef]

26. Habibi, Y.A.; Mousavi, M.; Nakata, K. Boosting visible-light photocatalytic performance of g-C_3N_4/Fe_3O_4 anchored with $CoMoO_4$ nanoparticles: Novel magnetically recoverable photocatalysts. *J. Photochem. Photobiol. A Chem.* **2019**, *368*, 120–136. [CrossRef]
27. Habibi, Y.A.; Mousavi, M. Deposition of $CuWO_4$ nanoparticles over g-C_3N_4/Fe_3O_4 nanocomposite: Novel magnetic photocatalysts with drastically enhanced performance under visible-light. *Adv. Powder Technol.* **2018**, *29*, 1379–1392. [CrossRef]
28. Mousavi, M.; Habibi, Y.A.; Pouran, S.R. Review on magnetically separable graphitic carbon nitride-based nanocomposites as promising visible-light-driven photocatalysts. *J. Mater. Sci. Mater. Electron.* **2018**, *29*, 1719–1747. [CrossRef]
29. Singh, V.P.; Mishra, D.; Kabachkov, E.N.; Shul'ga, Y.M.; Vaish, R. The characteristics of BiOCl/Plaster of Paris composites and their photocatalytic performance under visible light illumination for self-cleaning. *Mater. Sci. Energy Technol.* **2020**, *3*, 299–307. [CrossRef]
30. Singh, V.P.; Vaish, R. Hierarchical growth of BiOCl on SrO-Bi_2O_3-B_2O_3 glass-ceramics for self-cleaning applications. *J. Am. Ceram. Soc.* **2018**, *101*, 2901–2913. [CrossRef]
31. Zhao, J.; Pan, H.; He, X.; Wang, Y.; Gu, L.; Hu, Y.S.; Chen, L.; Liu, H.; Dai, S. Size-controlled synthesis and morphology evolution of bismuth trifluoride nanocrystals via a novel solvent extraction route. *Nanoscale* **2013**, *5*, 518–522. [CrossRef]
32. Feng, C.; Teng, F.; Liu, Z.; Chang, C.; Zhao, Y.; Wang, S.; Chen, M.; Yao, W.; Zhu, Y. A newly discovered BiF_3 photocatalyst with a high positive valence band. *J. Mol. Catal. A Chem.* **2015**, *401*, 35–40. [CrossRef]
33. Yang, Z.; Wang, X.; Liu, L.; Yang, S.; Su, X. First-principles calculations on structural, magnetic and electronic properties of oxygen doped BiF_3. *Comput. Mater. Sci.* **2011**, *50*, 3131–3135. [CrossRef]
34. Lei, S.; Wang, C.; Cheng, D.; Gao, X.; Chen, L.; Yan, Y.; Zhou, J.; Xiao, Y.; Cheng, B. Hierarchical BiF_3-Bi_2NbO_5F core-shell structure and its application in the photosensitized degradation of rhodamine B under visible light irradiation. *J. Phys. Chem. C* **2015**, *119*, 502–511. [CrossRef]
35. Sarkar, S.; Dash, A.; Mahalingam, V. Strong stokes and upconversion luminescence from ultrasmall Ln^{3+}-doped BiF_3 (Ln=Eu^{3+}, Yb^{3+}/Er^{3+}) nanoparticles confined in a polymer matrix. *Chem. Asian J.* **2014**, *9*, 447–451. [CrossRef] [PubMed]
36. Kan, Y.; Teng, F.; Yang, Y.; Xu, J.; Yang, L. Direct conversion mechanism from BiOCl nanosheets to BiOF, $Bi_7F_{11}O_5$ and BiF_3 in the presence of a fluorine resource. *RSC Adv.* **2016**, *6*, 63347–63357. [CrossRef]
37. Yu, J.; Li, C.; Liu, S. Effect of PSS on morphology and optical properties of ZnO. *J. Colloid Interface Sci.* **2008**, *326*, 433–438. [CrossRef] [PubMed]
38. Mills, A.; Wang, J.; McGrady, M. Method of rapid assessment of photocatalytic activities of self-cleaning films. *J. Phys. Chem. B* **2006**, *110*, 18324–18331. [CrossRef] [PubMed]
39. Lu, H.; Ju, T.; She, H.; Wang, L.; Wang, Q. Microwave-assisted synthesis and characterization of BiOI/BiF_3 p–n heterojunctions and its enhanced photocatalytic properties. *J. Mater. Sci. Mater. Electron.* **2020**, *31*, 13787–13795. [CrossRef]
40. Yang, Y.; Teng, F.; Kan, Y.; Yang, L.; Liu, Z.; Gu, W.; Zhang, A.; Hao, W.; Teng, Y. Investigation of the charges separation and transfer behavior of BiOCl/BiF3heterojunction. *Appl. Catal. B Environ.* **2017**, *205*, 412–420. [CrossRef]
41. Ritika; Kaur, M.; Umar, A.; Mehta, S.K.; Kansal, S.K. BiF_3 octahedrons: A potential natural solar light active photocatalyst for the degradation of Rhodamine B dye in aqueous phase. *Mater. Res. Bull.* **2019**, *112*, 376–383. [CrossRef]
42. Zhang, S.; Chen, X.; Song, L. Preparation of BiF_3/BiOBr heterojunctions from microwave-assisted method and photocatalytic performances. *J. Hazard. Mater.* **2019**, *367*, 304–315. [CrossRef] [PubMed]
43. Sharma, S.K.; Singh, V.P.; Chauhan, V.S.; Kushwaha, H.S.; Vaish, R. Photocatalytic Active Bismuth Fluoride/Oxyfluoride Surface Crystallized $2Bi_2O_3$-B_2O_3 Glass–Ceramics. *J. Electron. Mater.* **2018**, *47*, 3490–3496. [CrossRef]
44. Singh, V.P.; Vaish, R. Controlled crystallization of photocatalytic active Bismuth oxyfluoride/Bismuth fluoride on SrO-Bi_2O_3-B_2O_3transparent glass ceramic. *J. Eur. Ceram. Soc.* **2018**, *38*, 3635–3642. [CrossRef]
45. Singh, G.; Singh, V.P.; Vaish, R. Controlled crystallization of BiOCl/BiF_3 on ZnO–Bi_2O_3–B_2O_3 glass surfaces for photocatalytic and self-cleaning applications. *Materialia* **2019**, *5*, 100196. [CrossRef]